

Structure-based design of small molecule inhibitors of the *cagT4SS*

ATPase Cag α of *Helicobacter pylori*

¹Claire Morin[#], ¹Vijay Tailor Verma[#], ¹Tarun Arya, ¹Bastien Casu, ²Eric Jolicoeur, ²Réjean Ruel

^{2,3}Anne Marinier, ¹Jurgen Sygusch and ¹Christian Baron*

¹Department of Biochemistry and Molecular Medicine, Faculty of Medicine,

Université de Montréal, Québec, Canada

²Institut de Recherche en Immunologie et Cancérologie, Université de Montréal, Québec, Canada

and

³Department of Chemistry, Faculty of Arts and Sciences

Université de Montréal, Québec, Canada

Keywords: *Helicobacter pylori*, *cagPAI*, Cag α , VirB11, ATPase, anti-virulence, type IV secretion system, pili, inhibitors

*Corresponding author

[#]The first two authors made equal contributions to this work

Abstract

We here describe the structure-based design of small molecule inhibitors of the type IV secretion system of *Helicobacter pylori*. The secretion system is encoded by the *cag* pathogenicity island, and we chose Cag α , a hexameric ATPase and member of the family of VirB11-like proteins, as target for inhibitor design. We first solved the crystal structure of Cag α in a complex with the previously identified small molecule inhibitor 1G2. The molecule binds at the interface between two Cag α subunits and mutagenesis of the binding site identified Cag α residues F39 and R73 as critical for 1G2 binding. Based on the inhibitor binding site we synthesized 98 small molecule derivatives of 1G2 to improve binding of the inhibitor. We used the production of interleukin-8 of gastric cancer cells during *H. pylori* infection to screen the potency of inhibitors and we identified five molecules (1G2_1313, 1G2_1338, 1G2_2886, 1G2_2889 and 1G2_2902) that have similar or higher potency than 1G2. Differential scanning fluorimetry suggested that these five molecules bind Cag α , and enzyme assays demonstrated that some are more potent ATPase inhibitors than 1G2. Finally, scanning electron microscopy revealed that 1G2 and its derivatives inhibit the assembly of T4SS-determined extracellular pili suggesting a mechanism for their anti-virulence effect.

Introduction

Helicobacter pylori (*H. pylori*) is a Gram-negative bacterium isolated from gastric samples in the 1980s by Warren and Marshall. They demonstrated that the stomach is not sterile and that *H. pylori* causes inflammatory disease while colonizing the stomach (1). It was subsequently shown that chronic *H. pylori* colonization leads to gastric disease like ulcer, gastric adenocarcinoma and stomach cancer (2–4). *H. pylori* has been associated with humans for more than 1000 years and analysis of a strain from a human 5,300 years-old iceman showed a high degree of similarity with today's *H. pylori* strains (5). Up to 50 to 90% of the human population is colonized by *H. pylori* and its prevalence depend on the geographic localization of populations in the world (6,7). *H. pylori* carry a lot of difference virulence factors for the colonization of the stomach, for the establishment of a niche between epithelial cells of the stomach and others that cause inflammatory responses in human cells (2,8,9). The main virulence factors are the urease that neutralises the acidic environment, the vacuolating cytotoxin A (VacA) and the type IV secretion system (T4SS) (8–10). The T4SS comprises 27 proteins coded by the cytotoxin-associated gene (*cag*) pathogenicity island (*cagPAI*). The T4SS in *H. pylori* is used for the injection of the oncoprotein CagA as well as for the transfer of peptidoglycan fragments (11–14). CagA interferes with different metabolic pathways in gastric epithelial cells, leading to depolarisation of the cell, an increase of cell mobility and the loss of tight junctions (8,15–17). The resulting disorganization of gastric cell structure contributes to gastric disease (18–20). Not all *H. pylori* carry a *cagPAI*, but it is a major factor contributing to gastric disease and cancer (20).

Antibiotic therapy is commonly used for the treatment of patients with gastric disease. The treatment comprises triple or quadruple therapy and often includes proton pump inhibitors and

bismuth salts (21–25). Therapy with multiple antibiotics provokes a high selection pressure for antibiotic resistance. In addition, *H. pylori* is highly transformable, and it can acquire resistance that spreads in the environment. Over the last 10 years more than half of *H. pylori* patient isolates were found to carry at least one resistance gene against the first line antibiotics (26–28). In 2017 the World Health Organization published a report underlining the emergency of finding new antibiotics against *H. pylori* (29).

Considering the rise of antibiotic resistance, alternative therapeutic methods to fight bacterial infections have emerged that may not lead to strong selection pressure (30–33). Targeting virulence factors that are not essential for bacterial survival is one of the investigated approaches (34–37). *H. pylori* virulence factors such as the T4SS are not essential for its survival, but they are major contributors to severe gastric disease. The *cag*T4SS proteins are unique to *H. pylori* and inhibitors would therefore not target other bacteria of the microbiome. We have chosen the essential ATPase Cag α as a target (14,38,39). Cag α is a hexameric ATPase that localizes at the inner membrane and is a homolog of VirB11 proteins that are conserved and essential for all T4SS.

Previously, we have used fragment-based screening to identify small molecules that interact with Cag α and we identified 1G2 as a non-competitive inhibitor of its ATPase activity (37). Here, we characterized the binding site by X-ray crystallography and mutagenesis identified critical amino acid residues. Based on the information of the binding site we created a family of 1G2 derivatives and some of them have interesting potential as inhibitors of T4SS activity and of extracellular assembly of Cag pili.

Materials and Methods

Cloning and mutagenesis

Cloning of Cag α was described by Arya *et al*, 2019 (37). The plasmid carrying the WT Cag α protein pHTCag α was amplified using the QuikChange II site-directed mutagenesis kit (Agilent) using 33 bp primers (suppl. Tab. 1) to introduce single codon mutations to change amino acid residues at the 1G2 binding site, followed by Sanger sequencing on an ABI 3730 sequencer.

Expression and purification of Cag α

The expression and of purification Cag α wild type and mutant proteins was conducted as previously described by Arya *et al*, 2019 (37).

Crystallisation and structure determination

Initial crystallization conditions were established using the MCSG screen from Anatrace (USA) using 6 mg/ml of Cag α and 1 mM of 1G2 (1:10 ratio). Final crystals were grown at room temperature using the hanging drop vapour diffusion method in 100 mM Bis-Tris (pH 6.5) and 2mM ammonium sulfate. Drops containing 2 μ L of protein-inhibitor-mixture (1:10 ratio) and 2 μ L of reservoir solution were incubated for 2 weeks. Hexagonally-shaped crystals appeared after 7-10 days. The crystals were cryo-protected in 100 mM Tris-HCl buffer (pH 8.5), 2 M ammonium sulfate and 25% glycerol, flash frozen in liquid nitrogen and the data were collected at microfocus beamline F1 at the Cornell High Energy Synchrotron Source (CHESS). The intensity data was processed using the HKL2000(40) program (suppl. Tab. 2) . The structure was solved by molecular replacement using the coordinates of PDB ID: 1G6O as search model.

Refinement and modeling were performed using REFMAC and Coot (41,42). Final graphical figures and tables were generated using the Pymol-integrated Phenix software suite (43). The structure was published in the PDB (PDB code: 6BGE, <https://www.rcsb.org/structure/6BGE>).

Docking of 1G2 and derivatives to CagA

Autodoc Vina was used for binding energy calculations. The CagA structure used for the binding from PDB 1G6O (RCSB PDB - 1G6O: CRYSTAL STRUCTURE OF THE HELICOBACTER PYLORI ATPASE, H. PYLORI0525, IN COMPLEX WITH ADP) was used for docking.

Differential scanning fluorimetry (DSF)

To assess binding of 1G2 derivatives to CagA and its mutant proteins, DSF was used in the presence of SYPRO orange as in Arya *et al*, 2019 (37).

Synthesis of the 1G2 derivatives

The organic reagents are prepared as DMF solutions: Solution 1 : The heteroaryl halide building blocks solution was prepared by weighing 1.77 mmol in a 2 ml vial. DMF was added and the volume is adjusted to 400 μ l. Solution 2 : The scaffold (methyl-4-hydroxybenzoate) was weighed (1259 mg; 8.27 mmol) in a 40 ml vial, the solid was dissolved with DMF and the volume adjusted to 29.4 ml. A 0.6-2 ml microwave vial was added with 161 mg (0.493 mmol; 2.5 eq.) of Cs₂CO₃, equipped with a stirbar, charged with the heteroaryl halide solution (100 μ l; 2.25 eq.) followed by scaffold solution (700 μ l; limiting reagent). The suspension was transferred to a Biotage Initiator microwave reactor to run the reactions at 180 °C for 1 h. The reaction was monitored by liquid chromatography mass spectrometry (LCMS). The reaction mixtures were

filtered on a filtering plate (96 deep-well plate; PE Frit 25 mm; Long drip; 2 ml) using a MeOH/DMSO (2:1) mixture. Filtration was forced using HT4X Genevac for centrifugal filtration. The filtered mixtures were added to 50 ml of AcOH (pH adjusted <5) and purified on a reverse-phase Kinetex 5 μ m C18 column 21.2 x 100 mm and was eluted with MeOH - Water - 0.1% AcOH. Gradient: Isocratic 25 or 30 % for 1.5 minutes then gradient to 100% MeOH over 8.5 minutes. Tubes containing the desired compounds were identified and placed on an HT6-Genevac evaporator. After removal of the solvent, the content of the tubes was transferred to pre-tared 4 ml vials using a (1:1) DCM:MeOH mixture. The vials were placed in a HT6 Genevac evaporator and the solvents removed under reduced pressure, followed by NMR and LCMS analysis.

Enzyme activity assay

The ATPase activity was quantified using a malachite green binding assay (37). The 100 μ L reaction mixtures contained 60 nM of enzyme, 25 mM HEPES (pH 7.5), 100 mM NaCl, 200 μ M MgCl₂ and 200 μ M of 1G2 derivative. The reaction mixtures were incubated for 15 min at 30 °C. After incubation, ATP was added at 100 μ M concentration and incubated again for 30 minutes at 30 °C and then 40 μ L of malachite green assay mixture was added. The formation of the blue phosphomolybdate-malachite green complex was in linear relation to the amount of released inorganic phosphate and measured at 610 nm. Color generated was estimated compared to series of standards.

IC₅₀ determination

IC₅₀ values were determined by incubating different concentrations of molecules (5–2,500 μM; from stocks of 100 mM) with enzyme in 25 mM HEPES (pH 7.5) and 100 mM NaCl and 200 μM of MgCl₂. Mixtures were incubated with inhibitors for 15 min, followed by addition of ATP and incubation for 30 min at 37°C. The reactions were stopped by addition of 40 μl malachite green solution and the inorganic phosphate released was determined at 610 nm. Data were plotted as 1/rate versus inhibitor concentration for each substrate concentration and a linear fit was calculated by non-linear regression using SigmaPlot (version 11.0).

Bacterial strains, cell lines and culture conditions

H. pylori strain 26695 (ATCC700392) was used as a positive control, and the previously described $\Delta cagV$ (*H. pylori*0530) mutant recreated in our laboratory was used as negative control (37,44). All the strains were cultivated on Columbia agar base (BD) containing 10% (v/v) horse serum (Wisent Inc.), 5% (v/v) laked horse Blood (Wisent Inc.) with β -cyclodextrin (2 mg/mL), vancomycin (10 mg/ml) and amphotericin B (10 mg/ml). Chloramphenicol (34 mg/ml) was added in case of the $\Delta cagV$ strain to select for the chloramphenicol (*cam*) gene cassette used to disrupt the gene. For liquid cultures, brain heart infusion (BHI) media (Oxoid) was supplemented with 10% fetal bovine serum (FBS) and appropriate antibiotics. Bacteria were cultivated at 37°C under microaerophilic conditions (5% oxygen, 10% CO₂). Gastric human cells (AGS CRL-1739) cells were grown at 37°C in F12K media (Wisent Inc.) with 10% (v/v) FBS (Wisent Inc.) in a 5% CO₂-containing atmosphere.

Cell proliferation Assay

AGS cells cultivated at 5×10^4 cells/well density were incubated overnight with 100 μM of molecules at 37°C in a 5% CO_2 -containing atmosphere. The cell proliferation was evaluated using the Cell Proliferation Reagent WST-1 (CELLPRO-RO, Roche).

Infection of AGS by H. pylori strains and IL-8 production

AGS cells cultivated at 7×10^5 cells/well density in 6-well plates were infected for 4h or 0.3×10^5 cell/well density in a microplate for 1h, with a culture of *H. pylori* at multiplicity of infection (MOI) 1:100. *H. pylori* were first pre-incubated for 1h in F12K supplement with 10% FBS with or without 1G2 at concentration $200 \mu\text{M}$ at 37°C in a 5% CO_2 -containing atmosphere. After 4h infection under microaerophilic conditions, supernatants were sampled and centrifuged at 15,000 g to remove cells and debris; the supernatants were conserved at -20°C . The level of IL-8 in cell culture supernatants was determined using a human IL-8 ELISA kit (Invitrogen).

Sample preparation and western blotting

After 4h of infection, the cells were washed with phosphate-buffered saline (Wisent Inc.) and lysed in RIPA Buffer (50 mM Tris-HCl pH 8.0, 150 mM sodium chloride, 1.0% Igepal CA-630 NP-40, 0.5% sodium deoxycholate, 0.1% sodium dodecyl sulfate), complemented with a protease inhibitor cocktail for mammalian tissues (Sigma Aldrich) and a phosphatase inhibitor cocktail for tyrosine protein phosphatases, acid and alkaline phosphatases (Sigma Aldrich). The cells were harvested, incubated at 95°C for 5 min with SDS-PAGE sample buffer and centrifuged for 10 min at 10,000 rpm, followed by SDS-PAGE and western blotting. The production of proteins was assessed with monoclonal mouse anti-*Helicobacter pylori* CagA (HyTest Ltd.) and rabbit Cag α antiserum (Abcam). The actin was identified using the anti- β -Actin antibody (C4): m-IgG Fc BP-

HRP (Santa Cruz, sc-528515). The secondary antibodies (rabbit and mouse) were purchased from Biorad and the HRP signal was developed using Clarity Western ECL Substrate (Biorad).

Scanning electron microscopy

AGS cells were cultivated on round cover glasses (Fisherbrand) at 6×10^5 cells/well density in 6-well plates. The cells were infected with *H. pylori* for 4h as explained above, washed with cold phosphate buffer (PB 0.1 M), fixed in 4% paraformaldehyde/0.1% glutaraldehyde for 30 min at 4°C, followed by another wash in PB. The samples were then incubated in osmium tetroxide 4% (0.1%) for 1 h at 4°C, followed by washing with PB. The samples were then dehydrated using a series of ethanol dilutions for 15 min each (30%, 50%, 70%, 80%, 90%, 95%, 100%, 100%), followed by drying using critical point dryer using the Leica EM CPD300. Then cells were then coated with 5 nm of carbon using the Leica EM ACE600. The sample were visualised using a Hitachi Regulus 8220 scanning electron Microscope. The length and number of T4SS pili were measured using ImageJ software (45).

Statistical analysis

All the statistical analyses were performed using GraphPad Prism 9 (9.5.1). T-test and ANOVA (Kruskal-Wallis test and ordinary One-way) were used to analyse the number of pili and their size, respectively.

Results

X-ray analysis reveals the 1G2 binding site

In our previous work we identified 1G2 as a non-competitive inhibitor of Cag α and this molecule has interesting potential for development into an anti-virulence drug (37). As first step towards designing more effective 1G2 derivatives, we characterized the binding site by X-ray crystallography. Cag α was co-crystallized with 1G2, and we solved the X-ray structure of the Cag α -1G2 complex in the $P6_322$ crystal space group with two molecules in the asymmetric unit (Fig. 1A) to a resolution of 2.9 Å (suppl. Tab. 2). The structure was solved by molecular replacement using ADP bound Cag α (PDB code: 1G6O) as a search model. The overall structure of 1G2-bound Cag α (PDB code: 6BGE) is similar to that of the Cag α -ADP complex, but there are differences in interactions at the protein interface, and we identified the electron density of molecule 1G2 sandwiched between two Cag α molecules (Fig. 1A). The monomer structure of the Cag α -1G2 complex displays both N-terminal domain (NTD) and C-terminal domain (CTD) with nine α -helices labeled as $\alpha 1$ to $\alpha 9$ and 13 β -strands labeled as $\beta 1$ to $\beta 3$ (Fig. 1B). A structural overview from the top of the NTD reveals that 1G2 interacts with the NTD of both protein subunits (Fig. 1C). The 1G2 binding site is distinct from the active site to which ADP and the substrate analog ATP- γ -S bind (39,46). Molecule 1G2 binds to a hydrophobic pocket created by the interaction between the NTDs of two Cag α subunits and amino acids F68 and F39 make hydrophobic contacts with the two aromatic rings of the inhibitor. R73 and D69 are the amino acids involved in forming a polar contact with 1G2. R73 interacts with the pyridine ring via a hydrogen bond and the carboxylic group of 1G2 interacts with the backbone NH group of D69

forming a potential hydrogen bond (Fig. 1D). Sequence alignments with other Cag α /VirB11 homologs show that this site is not conserved suggesting that the molecule could likely be a specific inhibitor (suppl. Fig. 1).

Validation of the 1G2 binding site by mutagenesis of Cag α

To validate the binding site identified by X-ray crystallography (Fig. 1D) we mutagenized the *cag α* gene to change five amino acids at the binding site. We then purified the binding site mutants Cag α D38A, Cag α F39A, Cag α K41A, Cag α M42A, Cag α R73A, Cag α R73K and analysed their binding to 1G2 using differential scanning fluorimetry (DSF). This technique determines the melting temperature of a protein in a temperature gradient in the presence of the fluorescent dye SYPRO orange. Positive shifts are generally considered as evidence for binding due to stabilization by a small molecule (37). Analysis of the melting temperatures suggested that Cag α D38A and Cag α M42A bind 1G2 like the wild type protein whereas the binding of Cag α mutants F39A, K41A, R73A and R73K was reduced (Fig. 2A). These results suggest that Cag α residues F39, K41 and R73 contribute to binding of 1G2.

We next determined the ATPase activity of purified Cag α and its mutants using a malachite green assay measuring the release of inorganic phosphate from the ATP. All Cag α mutants have ATPase activities similar to the wild type protein and incubation with 1G2 at a concentration of 200 μ M reduced ATPase activity of most of them with the exception of Cag α R73A that was not inhibited (Fig. 2B). The effect of 1G2 on Cag α F39A, Cag α K41A and Cag α M42A was less pronounced than on the wild type protein. To gain more quantitative information on the effect of

1G2 on the different mutants we varied the concentration of the inhibitors and calculated IC_{50} values as a measure of inhibitor efficacy. The IC_{50} values for inhibition of the wild type and of Cag α D38A are in a similar range, those of Cag α K41A and Cag α M42A are significantly higher and Cag α F39A and Cag α R73A are resistant to the inhibitor (Fig. 2C). The enzyme assay results are consistent with those obtained by DSF suggesting that Cag α residues F39 and R73 are critically important for binding of 1G2 and that K41 and M42 also contribute to the effect of the inhibitor.

Design and selection of 1G2 derivatives molecules

Based on the results from co-crystallisation and mutagenesis of the active site we created a library of 96 1G2 derivatives by medicinal chemistry in an attempt to generate more potent inhibitors. We designed 1G2 derivatives to improve binding to amino acid residues at the inhibitor binding site and we also introduced functional groups that may modulate solubility and thereby permeation into cells (Fig. 3 and suppl. Fig. 3). The fact that a previously identified 1G2 derivative (1G2#4) (37) was more efficient against Cag α *in vitro* also informed this strategy since its additional methyl group may improve binding to K41. As first step to identify more potent 1G2 derivatives we screened for toxicity for human AGS (gastric adenocarcinoma) cells that are used for *H. pylori* infection experiments. Using a cell proliferation assay we identified four cytotoxic molecules, triggering more than 20% of mortality and these molecules were not further investigated. Next, we used a bacterial growth inhibition assay to test toxicity for *H. pylori* using an antibiogram-like technique with 200 μ M of 1G2 and derivatives (chloramphenicol as a

positive control) on filter plates and we found that none of the 92 derivatives is toxic for the bacteria (suppl. Tab. 4).

To determine the effect of the 1G2 derivatives on T4SS function we quantified the production of interleukin 8 (IL-8) during AGS cell infection by *H. pylori*. IL-8 is an inflammatory factor induced after co-infection with *H. pylori* and it provides a quantifiable readout since it is secreted into the cell culture supernatant (14). We designed a medium-throughput assay enabling us to measure the effects of preincubation of the molecules on IL-8 production of AGS cells in 96-well microtiter plates, followed by quantification using an ELISA assay. We conducted two rounds of screening to identify molecules that reduce IL-8 production more strongly than 1G2 in a reproducible fashion. The first round identified 25 molecules that cause similar or more pronounced reduction of IL-8 production (suppl. Fig. 2A) and a secondary screen identified five molecules (1G2_1313, 1G2_1338, 1G2_2886, 1G2_2889 and 1G2_2902) that lead to strong reductions of IL-8 induction in a reproducible fashion (Tab. 1 and suppl. Fig. 2B). The selected five molecules were further characterized using the infection model described by Arya *et al.* (37) and the assays were repeated six times to gain sufficient statistical power. To compare the effects of the molecules on the T4SS-dependent IL-8 induction, we subtracted the value of the control $\Delta cagV$ mutant strain, which represents the background on non-dependent T4SS IL-8 induction. We observed that 1G2 reduces IL-8 production to about 20% as compared to the wild type control without inhibitor. The five selected molecules have varying effect on IL-8 production. Molecules 1G2_2886, 1G2_2889 and 1G2_2902 have comparable effects to 1G2, but 1G2_1313 and 1G2_1338 reduce IL-8 production close to the background level of the $\Delta cagV$ mutant (Fig. 4).

Differential scanning fluorimetry and docking suggest that 1G2 derivatives bind Cagα

To characterize the five selected 1G2 derivatives we first tested their binding to Cag α using the DSF approach as above. Molecules 1G2_1313, 1G2_2889 and 1G2_2902 increased the melting temperature to a lower extent than 1G2, 1G2_2886 had a similar effect as compared to 1G2 and 1G2_1338 actually decreased the melting temperature (Fig. 5). We also conducted *in silico* docking using Autodock Vina software (47). This approach enables a computational prediction of the binding energies and the negative value obtained for 1G2 (-6.6 Δ G/mol) is consistent with its binding to Cag α (suppl. Tab. 3). The predicted binding energies for the five 1G2 derivatives (1G2_1313, 1G2_1338, 1G2_2886, 1G2_2889 and 1G2_2902) had more pronouncedly negative values (-9 to -10.2 Δ G/mol) suggesting that they may have higher affinities for Cag α than 1G2. Whereas the DSF results are not consistent with higher affinity of the 1G2 derivatives to Cag α the docking results suggest stronger binding and we tested their effects on enzyme activity next.

Effect of 1G2 derivatives molecules on the ATPase activity of Cagα

Using the malachite green assay as above we assessed to which degree the five 1G2 derivatives impact the enzymatic activity of Cag α . All molecules reduce the Cag α ATPase activity to varying degrees when they were applied at 500 μ M concentration (Fig. 6A). We then tested the inhibitors at varying concentrations and the IC₅₀ value of molecule 1G2_1313 is similar to that of 1G2 (256 μ M). In contrast, molecules 1G2_1338 (60 μ M), 1G2_2886 (47.50 μ M), 1G2_2889 (96 μ M) and 1G2_2902 (85 μ M) have lower IC₅₀ values than 1G2. These results are consistent with the

increased negative effects of these derivatives observed in the IL-8 production assay (Fig. 4) and further support the notion that these derivatives are more potent than 1G2.

1G2 and derivatives affect the assembly of T4SS pili

Finally, we tested the effects of 1G2 and its five derivatives on the physiology of the T4SS. AGS cells were infected with *H. pylori* wild type strain 26695 that had been pre-incubated with 200 μ M of the molecules, followed by infection of 4 hours and analysis of the cells. First, the presence of Cag proteins was analysed using western blotting to determine whether 1G2 and its derivatives have negative impacts on T4SS expression or stability. We do not observe any significant and reproducible effects on the amounts of the translocated virulence factor CagA or of the target Cag α suggesting that the inhibitors do not destabilize the T4SS (suppl. Fig. 4). Second, we used a recently developed quantifiable approach to analyze the T4SS-dependent assembly of extracellular pili using scanning electron microscopy (SEM) during AGS cell infection (Oudouhou and Morin, *et al*, 2023 submitted) (Fig. 7A). We observe on average of 17 (\pm 8) T4SS pili on the wild type strain in the absence of 1G2 and very few on the T4SS-defective Δ cagV strain 1 (\pm 2)(Fig. 7B). In contrast, in the presence of 1G2 we observe on average 3(\pm 3) T4SS-pili on the wild type strain and all 1G2 derivatives have similar strong inhibitory effects on pilus assembly (Fig. 7B). These results confirm that 1G2 and its derivatives have strong negative effects on T4SS pilus assembly, and it will be interesting to gain more detailed insights into the molecular mechanism of these molecules in future.

Discussion

The eradication therapies of *H. pylori* using antibiotics induce a high selection pressure leading to the acquisition of antibiotic resistance that can be transmitted between different strains and other members of the microbiome (24,48–51). Targeting the nonessential virulence factors that the bacteria use to infect the host is an alternative approach to reduce the pressure of selection induced by antibiotics (52–56). In this study we have characterized the binding site of Cag α inhibitor 1G2 using X-ray crystallography and mutagenesis suggesting a unique mechanism of inhibition via a binding site that is distinct from the ATPase active site. X-ray analysis suggested that five amino acids (D38, F39, K41, M42, R73) may form the 1G2 binding site. We mutated them individually and DSF as well as ATPase enzyme assays showed that F39 and R73 are critically important, and that K41 and M42 also contribute to the binding of 1G2. These data suggest that we have identified the 1G2 binding site and that it functions as an inhibitor of ATPase activity by not directly interfering with substrate binding.

Based on the information gained on the inhibitor binding site we synthesized a series of 98 1G2 derivatives that may have improved binding to amino acids at the binding site and/or penetration into the cells. We tested their toxicity for mammalian cells first to focus our efforts on molecules that do not interfere with other metabolic pathways in mammalian cells (57). In the spirit of our overall anti-virulence strategy, we also validated that these molecules are not toxic for *H. pylori*. We then screened the effects of 1G2 derivatives in a cell-based infection assay monitoring IL-8 production as a readout of T4SS activity to identify more potent anti-virulence molecules. Using this approach, we aimed at identifying 1G2 derivatives that have increased potency for the inhibition of Cag α and/or improved capacity to penetrate into the cells. This strategy was

informed by previously identified derivative 1G2#4 that was more active as an inhibitor of Cag α ATPase activity *in vitro* than 1G2 (IC₅₀ of 82 μ M as compared to 196 μ M), but the molecule was inactive as an inhibitor of IL-8 production (37), likely due to solubility issues. This molecule carries an additional methyl group that may form additional hydrophobic interactions with the carbon chain of K41. Using screening of IL-8 production instead of inhibition of ATPase activity as a readout we avoided the identification of molecules like 1G2#4 that are more potent enzyme inhibitors, but inactive as inhibitors of the pathogen.

We then characterized the *in vitro* activity of the five molecules that have the strongest negative effects on IL-8 production as compared to 1G2 (1G2_1313, 1G2_1338, 1G2_2886, 1G2_2889 and 1G2_2902). Interestingly, when we used DSF as an estimate for binding to the target Cag α , none of the molecules led to stronger positive shifts of the melting temperature than 1G2. This suggests that the improved inhibitory activity in the IL-8 production assay is not necessarily due to stronger binding to the target. Interestingly, molecule 1G2_1338 decreased the melting temperature in the DSF assay suggesting that it may have a distinct effect on its target than 1G2. Analysis of the effects of the 1G2 derivatives on Cag α ATPase activity revealed that four of them are in fact more potent inhibitors than 1G2 (1G2_1338: 60 μ M, 1G2_2886: 47 μ M, 1G2_2889: 96 μ M, 1G2_2902: 85 μ M). These values are in the range of what we observed previously for 1G2#4, and in addition these molecules are potent inhibitors of IL-8 production reducing this readout of T4SS activity to baseline level of a Cag protein deletion mutant in the case of 1G2_1338. In addition, like 1G2, the five derivatives strongly reduce the production of extracellular T4SS pili suggesting that they share the same overall mechanism of inhibition.

The molecules identified here are the result of a first round of synthesis in the context of a structure-activity relationship (SAR) study and some are already more potent than 1G2 as enzyme inhibitors or in the IL-8 inhibition assay. The results of this work will inform future rounds of optimization by medicinal chemistry to synthesize molecules that have potential for development into drugs. In addition, since these molecules are inhibitors of the assembly of extracellular T4SS pili they could be applied for mechanistic studies of the T4SS assembly and translocation process. Small molecule inhibitors could be applied to block T4SS at different stages of the infection process enabling us to determine the time at which pilus assembly and effector translocation from *H. pylori* to mammalian cells are required.

Acknowledgements

This work was supported by grants from the Cancer Research Society, the Charles Bowers Memorial Fund, the Bergeron-Jetté Foundation (CRS, #23404 and #25102) and the Natural Sciences and Engineering Research Council (NSERC, #RGPIN-2017-05123) to C.B. We are grateful to Dr. Dainelys Guadarrama Bell and other members of Dr. Antonio Nanci's laboratory at the Université de Montréal electron microscopy facility for technical support and assistance. Synchrotron X-ray data were collected at the Cornell High Energy Synchrotron Source (CHESS, MacCHESS beamline F1).

References

1. Marshall B, Warren JR. UNIDENTIFIED CURVED BACILLI IN THE STOMACH OF PATIENTS WITH GASTRITIS AND PEPTIC ULCERATION. *The Lancet*. juin 1984;323(8390):1311-5.
2. Amieva M, Peek RM. Pathobiology of *Helicobacter pylori*-Induced Gastric Cancer. *Gastroenterology*. janv 2016;150(1):64-78.
3. Coussens LM, Werb Z. Inflammation and cancer. *Nature*. déc 2002;420(6917):860-7.
4. Blaser N, Backert S, Pachathundikandi SK. Immune Cell Signaling by *Helicobacter pylori*: Impact on Gastric Pathology. In New York, NY: Springer US; 2019 [cité 10 mai 2019]. Disponible sur: http://link.springer.com/10.1007/5584_2019_360
5. Maixner F, Krause-Kyora B, Turaev D, Herbig A, Hoopmann MR, Hallows JL, et al. The 5300-year-old *Helicobacter pylori* genome of the Iceman. *Science*. 8 janv 2016;351(6269):162-5.
6. Hooi JKY, Lai WY, Ng WK, Suen MMY, Underwood FE, Tanyingoh D, et al. Global Prevalence of *Helicobacter pylori* Infection: Systematic Review and Meta-Analysis. *Gastroenterology*. août 2017;153(2):420-9.
7. Breckan RK, Paulssen EJ, Asfeldt AM, Kvamme JM, Straume B, Florholmen J. The All-Age Prevalence of *Helicobacter pylori* Infection and Potential Transmission Routes. A Population-Based Study. *Helicobacter*. déc 2016;21(6):586-95.
8. Ansari S, Yamaoka Y. *Helicobacter pylori* Virulence Factor Cytotoxin-Associated Gene A (CagA)-Mediated Gastric Pathogenicity. *Int J Mol Sci*. 8 oct 2020;21(19):7430.
9. Argent RH, Thomas RJ, Letley DP, Rittig MG, Hardie KR, Atherton JC. Functional association between the *Helicobacter pylori* virulence factors VacA and CagA. *J Med Microbiol*. 1 févr 2008;57(2):145-50.
10. Sharndama HC, Mba IE. *Helicobacter pylori*: an up-to-date overview on the virulence and pathogenesis mechanisms. *Braz J Microbiol*. mars 2022;53(1):33-50.
11. Backert S, Tegtmeyer N, Selbach M. The Versatility of *Helicobacter pylori* CagA Effector Protein Functions: The Master Key Hypothesis: The Versatility of *H. pylori* CagA. *Helicobacter*. juin 2010;15(3):163-76.
12. Backert S, Tegtmeyer N, Fischer W. Composition, structure and function of the *Helicobacter pylori* *cag* pathogenicity island encoded type IV secretion system. *Future Microbiol*. juin 2015;10(6):955-65.
13. Costa TRD, Harb L, Khara P, Zeng L, Hu B, Christie PJ. Type IV secretion systems: Advances in structure, function, and activation. *Mol Microbiol*. mars 2021;115(3):436-52.

14. Cover TL, Lacy DB, Ohi MD. The *Helicobacter pylori* Cag Type IV Secretion System. *Trends Microbiol.* août 2020;28(8):682–95.
15. Jang S, Hansen LM, Su H, Solnick JV, Cha JH. Host immune response mediates changes in *cagA* copy number and virulence potential of *Helicobacter pylori*. *Gut Microbes.* 31 déc 2022;14(1):2044721.
16. Freire de Melo F, Marques HS, Rocha Pinheiro SL, Lemos FFB, Silva Luz M, Nayara Teixeira K, et al. Influence of *Helicobacter pylori* oncoprotein CagA in gastric cancer: A critical-reflective analysis. *World J Clin Oncol.* 24 nov 2022;13(11):866–79.
17. Cheok YY, Lee CYQ, Cheong HC, Vadivelu J, Looi CY, Abdullah S, et al. An Overview of *Helicobacter pylori* Survival Tactics in the Hostile Human Stomach Environment. *Microorganisms.* 3 déc 2021;9(12):2502.
18. Yang L, Ying X, Liu S, Lyu G, Xu Z, Zhang X, et al. Gastric cancer: Epidemiology, risk factors and prevention strategies. *Chin J Cancer Res.* 2020;32(6):695–704.
19. Kalisperati P, Spanou E, Pateras IS, Korkolopoulou P, Varvarigou A, Karavokyros I, et al. Inflammation, DNA Damage, *Helicobacter pylori* and Gastric Tumorigenesis. *Front Genet* [Internet]. 27 févr 2017 [cité 24 févr 2023];8. Disponible sur: <http://journal.frontiersin.org/article/10.3389/fgene.2017.00020/full>
20. Salvatori S, Marafini I, Laudisi F, Monteleone G, Stolfi C. *Helicobacter pylori* and Gastric Cancer: Pathogenetic Mechanisms. *Int J Mol Sci.* 2 févr 2023;24(3):2895.
21. Ford AC, Gurusamy KS, Delaney B, Forman D, Moayyedi P. Eradication therapy for peptic ulcer disease in *Helicobacter pylori* -positive people. Cochrane Upper GI and Pancreatic Diseases Group, éditeur. *Cochrane Database Syst Rev* [Internet]. 19 avr 2016 [cité 29 juin 2020]; Disponible sur: <http://doi.wiley.com/10.1002/14651858.CD003840.pub5>
22. Gatta L, Vakil N, Vaira D, Scarpignato C. Global eradication rates for *Helicobacter pylori* infection: systematic review and meta-analysis of sequential therapy. *BMJ.* 7 août 2013;347(aug07 1):f4587–f4587.
23. Zhang Y, Suo B, Tian X, Zhang H, Lu H, Yao X, et al. New regimens as first-line eradication therapy for *Helicobacter pylori* infection in patients allergic to penicillin: A randomized controlled trial. *Helicobacter* [Internet]. 8 févr 2023 [cité 14 févr 2023]; Disponible sur: <https://onlinelibrary.wiley.com/doi/10.1111/hel.12956>
24. Katelaris P, Hunt R, Bazzoli F, Cohen H, Fock KM, Gemilyan M, et al. *Helicobacter pylori* World Gastroenterology Organization Global Guideline. *J Clin Gastroenterol.* févr 2023;57(2):111–26.
25. Mansour-Ghanaei F, Samadi A, Joukar F, Tirgar Fakheri H, Hassanipour S, Ashoobi MT, et al. Efficacy and tolerability of fourteen-day sequential quadruple regimen: pantoprazole, bismuth, amoxicillin, metronidazole and or furazolidone as first-line therapy for eradication of *Helicobacter pylori*: a randomized, double-blind clinical trial. *EXCLI J* 18Doc644 ISSN 1611-

- 2156 [Internet]. 2019 [cité 31 oct 2019]; Disponible sur: https://www.excli.de/vol18/Mansour-Ghanaei_19082019_proof.pdf
26. Argueta EA, Alsamman MA, Moss SF, D'Agata EMC. Impact of antimicrobial resistance rates on eradication of *Helicobacter pylori* in a United States population. *Gastroenterology*. févr 2021;S0016508521004017.
 27. Boyanova L, Hadzhiyski P, Kandilarov N, Markovska R, Mitov I. Multidrug resistance in *Helicobacter pylori*: current state and future directions. *Expert Rev Clin Pharmacol* [Internet]. 19 août 2019 [cité 21 août 2019]; Disponible sur: <https://www.tandfonline.com/doi/full/10.1080/17512433.2019.1654858>
 28. Contreras-Omaña R, Escorcia-Saucedo AE, Velarde-Ruiz Velasco JA. Prevalence and impact of antimicrobial resistance in gastrointestinal infections: A review. *Rev Gastroenterol México Engl Ed*. juin 2021;S2255534X21000633.
 29. Tacconelli E, Carrara E, Savoldi A, Harbarth S, Mendelson M, Monnet DL, et al. Discovery, research, and development of new antibiotics: the WHO priority list of antibiotic-resistant bacteria and tuberculosis. *Lancet Infect Dis*. mars 2018;18(3):318-27.
 30. Dieye Y, Nguer CM, Thiam F, Diouara AAM, Fall C. Recombinant *Helicobacter pylori* Vaccine Delivery Vehicle: A Promising Tool to Treat Infections and Combat Antimicrobial Resistance. *Antibiotics*. 25 nov 2022;11(12):1701.
 31. Sathianarayanan S, Ammanath AV, Biswas R, B A, Sukumaran S, Venkidasamy B. A new approach against *Helicobacter pylori* using plants and its constituents: A review study. *Microb Pathog*. juill 2022;168:105594.
 32. Frost I, Sati H, Garcia-Vello P, Hasso-Agopsowicz M, Lienhardt C, Gigante V, et al. The role of bacterial vaccines in the fight against antimicrobial resistance: an analysis of the preclinical and clinical development pipeline. *Lancet Microbe*. févr 2023;4(2):e113-25.
 33. Zhang Y, Li X, Shan B, Zhang H, Zhao L. Perspectives from recent advances of *Helicobacter pylori* vaccines research. *Helicobacter* [Internet]. déc 2022 [cité 9 janv 2023];27(6). Disponible sur: <https://onlinelibrary.wiley.com/doi/10.1111/hel.12926>
 34. Escaich S. Antivirulence as a new antibacterial approach for chemotherapy. *Curr Opin Chem Biol*. août 2008;12(4):400-8.
 35. Hwang HJ, Choi H, Hong S, Moon HR, Lee JH. Antipathogenic Compounds That Are Effective at Very Low Concentrations and Have Both Antibiofilm and Antivirulence Effects against *Pseudomonas aeruginosa*. Oglesby AG, éditeur. *Microbiol Spectr* [Internet]. 8 sept 2021 [cité 21 sept 2021]; Disponible sur: <https://journals.asm.org/doi/10.1128/Spectrum.00249-21>
 36. Buß M, Tegtmeyer N, Schnieder J, Dong X, Li J, Springer TA, et al. Specific high affinity interaction of *Helicobacter pylori* CagL with integrin $\alpha_v \beta_6$ promotes type IV secretion of

CagA into human cells. FEBS J [Internet]. 14 juin 2019 [cité 18 juin 2019]; Disponible sur: <https://onlinelibrary.wiley.com/doi/abs/10.1111/febs.14962>

37. Arya T, Oudouhou F, Casu B, Bessette B, Sygusch J, Baron C. Fragment-based screening identifies inhibitors of ATPase activity and of hexamer formation of Cag α from the *Helicobacter pylori* type IV secretion system. *Sci Rep*. déc 2019;9(1):6474.
38. Haley KP, Blanz EJ, Gaddy JA. High Resolution Electron Microscopy of the *Helicobacter pylori* Cag Type IV Secretion System Pili Produced in Varying Conditions of Iron Availability. *J Vis Exp* [Internet]. 21 nov 2014 [cité 28 nov 2018];(93). Disponible sur: <http://www.jove.com/video/52122/high-resolution-electron-microscopy-helicobacter-pylori-cag-type-iv>
39. Yeo HJ, Savvides SN, Herr AB, Lanka E, Waksman G. Crystal Structure of the Hexameric Traffic ATPase of the *Helicobacter pylori* Type IV Secretion System. *Mol Cell*. déc 2000;6(6):1461–72.
40. Otwinowski Z, Minor W. [20] Processing of X-ray diffraction data collected in oscillation mode. In: *Methods in Enzymology* [Internet]. Elsevier; 1997 [cité 30 mai 2023]. p. 307–26. Disponible sur: <https://linkinghub.elsevier.com/retrieve/pii/S007668799776066X>
41. Emsley P, Cowtan K. *Coot*: model-building tools for molecular graphics. *Acta Crystallogr D Biol Crystallogr*. 1 déc 2004;60(12):2126–32.
42. Murshudov GN, Vagin AA, Dodson EJ. Refinement of Macromolecular Structures by the Maximum-Likelihood Method. *Acta Crystallogr D Biol Crystallogr*. 1 mai 1997;53(3):240–55.
43. Adams PD, Grosse-Kunstleve RW, Hung LW, Ioerger TR, McCoy AJ, Moriarty NW, et al. *PHENIX*: building new software for automated crystallographic structure determination. *Acta Crystallogr D Biol Crystallogr*. 1 nov 2002;58(11):1948–54.
44. Fischer W, Püls J, Buhrdorf R, Gebert B, Odenbreit S, Haas R. Systematic mutagenesis of the *Helicobacter pylori* cag pathogenicity island: essential genes for CagA translocation in host cells and induction of interleukin-8: Functional dissection of the *H. pylori* type IV secretion system. *Mol Microbiol*. 13 janv 2002;42(5):1337–48.
45. Schindelin J, Arganda-Carreras I, Frise E, Kaynig V, Longair M, Pietzsch T, et al. Fiji: an open-source platform for biological-image analysis. *Nat Methods*. juill 2012;9(7):676–82.
46. Savvides SN. VirB11 ATPases are dynamic hexameric assemblies: new insights into bacterial type IV secretion. *EMBO J*. 1 mai 2003;22(9):1969–80.
47. Trott O, Olson AJ. AutoDock Vina: Improving the speed and accuracy of docking with a new scoring function, efficient optimization, and multithreading. *J Comput Chem*. 2009;NA-NA.

48. Seo JW, Park JY, Shin TS, Kim JG. The analysis of virulence factors and antibiotic resistance between *Helicobacter pylori* strains isolated from gastric antrum and body. *BMC Gastroenterol* [Internet]. déc 2019 [cité 28 oct 2019];19(1). Disponible sur: <https://bmcgastroenterol.biomedcentral.com/articles/10.1186/s12876-019-1062-5>
49. Wang L, Yao H, Tong T, Lau K, Leung SY, Ho JWK, et al. Dynamic changes in antibiotic resistance genes and gut microbiota after *Helicobacter pylori* eradication therapies. *Helicobacter* [Internet]. 30 déc 2021 [cité 4 févr 2022]; Disponible sur: <https://onlinelibrary.wiley.com/doi/10.1111/hel.12871>
50. Kakiuchi T, Yamamoto K, Imamura I, Hashiguchi K, Kawakubo H, Yamaguchi D, et al. Gut microbiota changes related to *Helicobacter pylori* eradication with vonoprazan containing triple therapy among adolescents: a prospective multicenter study. *Sci Rep*. déc 2021;11(1):755.
51. Ye Q, Shao X, Shen R, Chen D, Shen J. Changes in the human gut microbiota composition caused by *Helicobacter pylori* eradication therapy: A systematic review and meta-analysis. *Helicobacter*. 9 juin 2020;e12713.
52. Hilleringmann M, Pansegrau W, Doyle M, Kaufman S, MacKichan ML, Gianfaldoni C, et al. Inhibitors of *Helicobacter pylori* ATPase Cag α block CagA transport and cag virulence. *Microbiology*. 1 oct 2006;152(10):2919–30.
53. He S, Almalki AA, Rafeeq MM, Sain ZM, Alqosaibi AI, Alnamshan MM, et al. Targeting Cytotoxin-Associated Antigen A, a Virulent Factor of *Helicobacter pylori*-Associated Gastric Cancer: Structure-Based In Silico Screening of Natural Compounds. *Molecules*. 23 janv 2022;27(3):732.
54. Sabino YNV, Cotter PD, Mantovani HC. Anti-virulence compounds against *Staphylococcus aureus* associated with bovine mastitis: A new therapeutic option? *Microbiol Res*. juin 2023;271:127345.
55. Suerbaum S, Coombs N, Patel L, Pscheniza D, Rox K, Falk C, et al. Identification of Antimotilins, Novel Inhibitors of *Helicobacter pylori* Flagellar Motility That Inhibit Stomach Colonization in a Mouse Model. *Rappuoli R, éditeur. mBio*. 26 avr 2022;13(2):e03755-21.
56. Yang D, Hao S, Zhao L, Shi F, Ye G, Zou Y, et al. Paeonol Attenuates Quorum-Sensing Regulated Virulence and Biofilm Formation in *Pseudomonas aeruginosa*. *Front Microbiol*. 4 août 2021;12:692474.
57. Ngo HX, Garneau-Tsodikova S. What are the drugs of the future? *MedChemComm*. 2018;9(5):757–8.

Figures

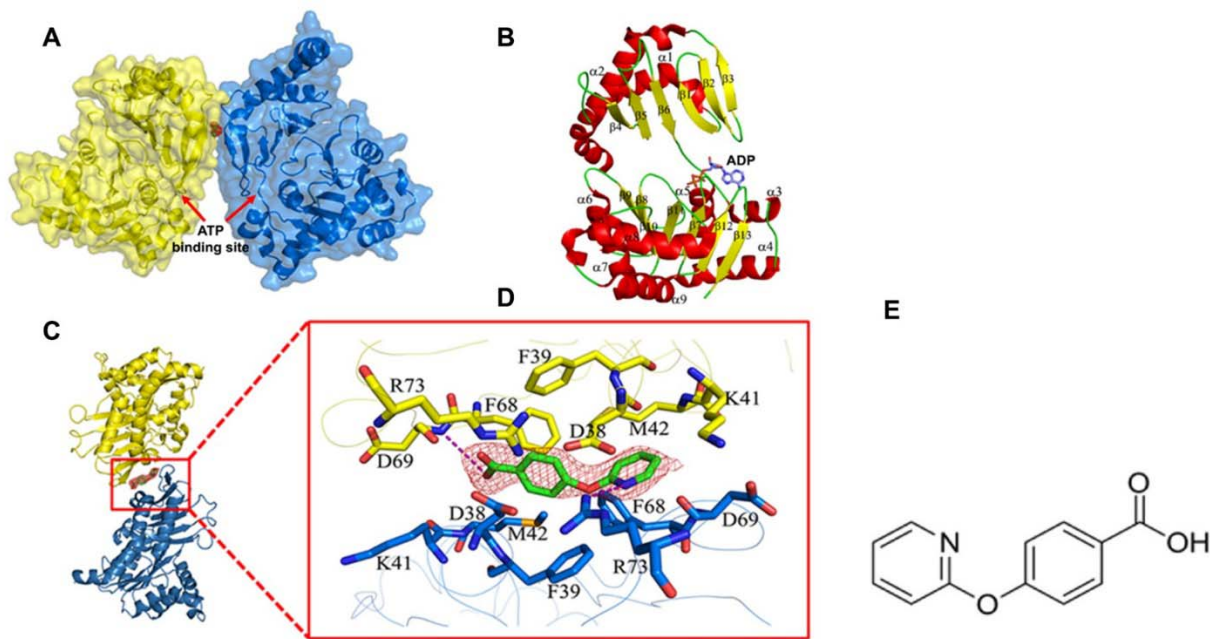


Figure 1: 1G2 Binding determined by X-ray crystallography. A) Cartoon representation of the crystal structure of Cag α crystallized as two molecules in the asymmetric unit. Red map in middle of two subunits represents molecule 1G2 and arrows indicate the ATP/ADP binding site. B) Representation of the monomeric subunit of Cag α in ribbon form: α helices, β strands and loops are represented in yellow, red and green, respectively. The nine helices are labeled as α 1 to α 9 and the β -strands are labeled as β 1 to β 13 and the ADP binding site is indicated. C) Side view of the interaction of two subunits of protein with 1G2 in the middle represented as green stick and red map. D) Enlarged view of 1G2 binding at the interface between two protein subunits. The 2FO-FC electron density map of 1G2 was contoured at 1.5σ . E) 2D structure of 1G2.

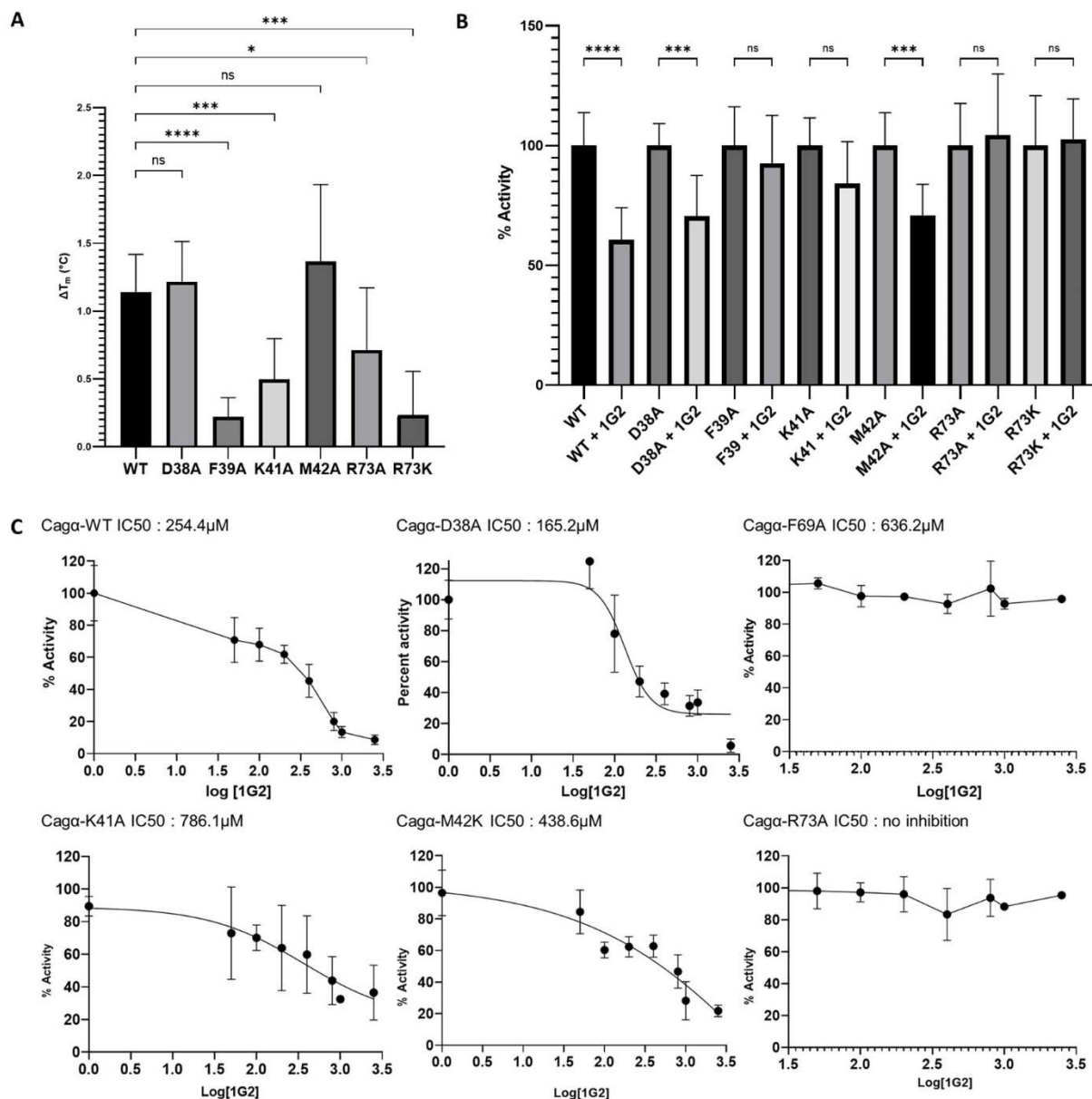


Figure 2: Characterization of active site mutants by differential scanning fluorimetry and ATPase enzyme assays. A) Changes in the melting temperature of Cag α mutant proteins were measured by DSF after incubation with molecules at 5 mM final concentration (n= 3 times triplicates). The results were analysed using ANOVA test ns ; non significant, * p<0.05 , *** p<0.001 , **** p<0.0001. B) Effect of 1G2 derivatives on the ATPase activity of Cag α mutant proteins. Cag α WT and mutant proteins were incubated with 1G2 at different concentrations and

ATPase activity was measured by malachite green assay, ANOVA test ns ; non significant, ***
p=<0.001 , **** p<0.0001. C) Dose-response curves of ATPase activity of mutant proteins
showing IC₅₀ values in the presence of 1G2. C) Dose-response curves of ATPase activity of
mutant proteins showing IC₅₀ values in the presence of 1G2.

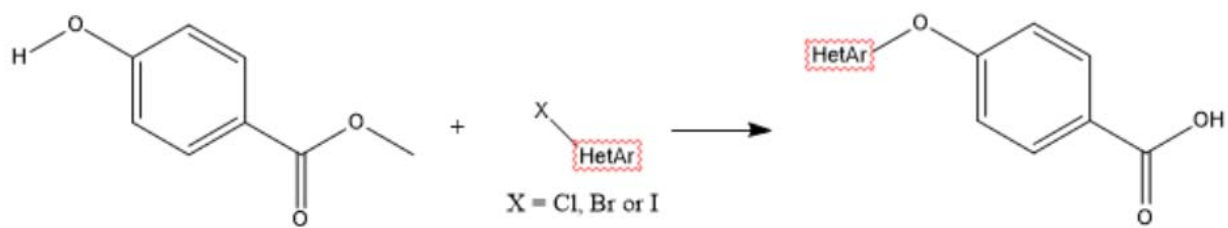


Figure 3: Synthesis of 1G2 derivatives See also suppl. Fig. 3.

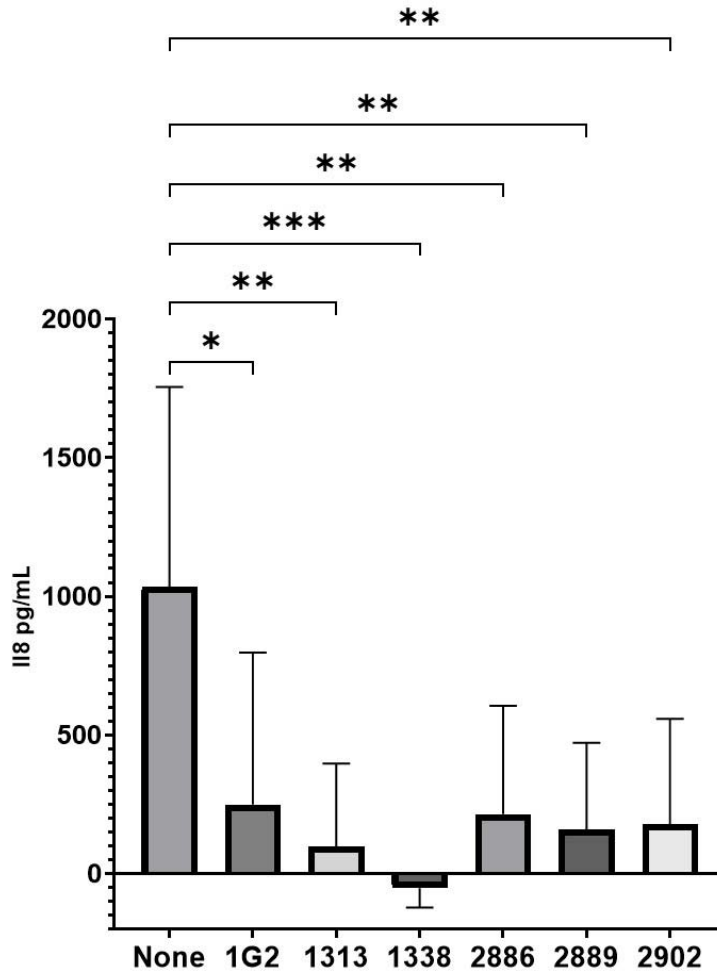


Figure 4: Quantification of the interleukin-8 production by AGS cells infected by *H. pylori* strains after treatment with the 1G2 and its derivatives. AGS cells were infected by the strain 26695 that had been preincubated with 200 μ M of molecules for 4 h and the amount of secreted IL-8 was measured by ELISA. The T4SS dependent induction of IL-8 is displayed in pg/ml (n=6) and the value for strain Δ cagV were used as baseline. *p<0.01, ** p<0.001, ***p<0.0005, , Ordinary one-way ANOVA test

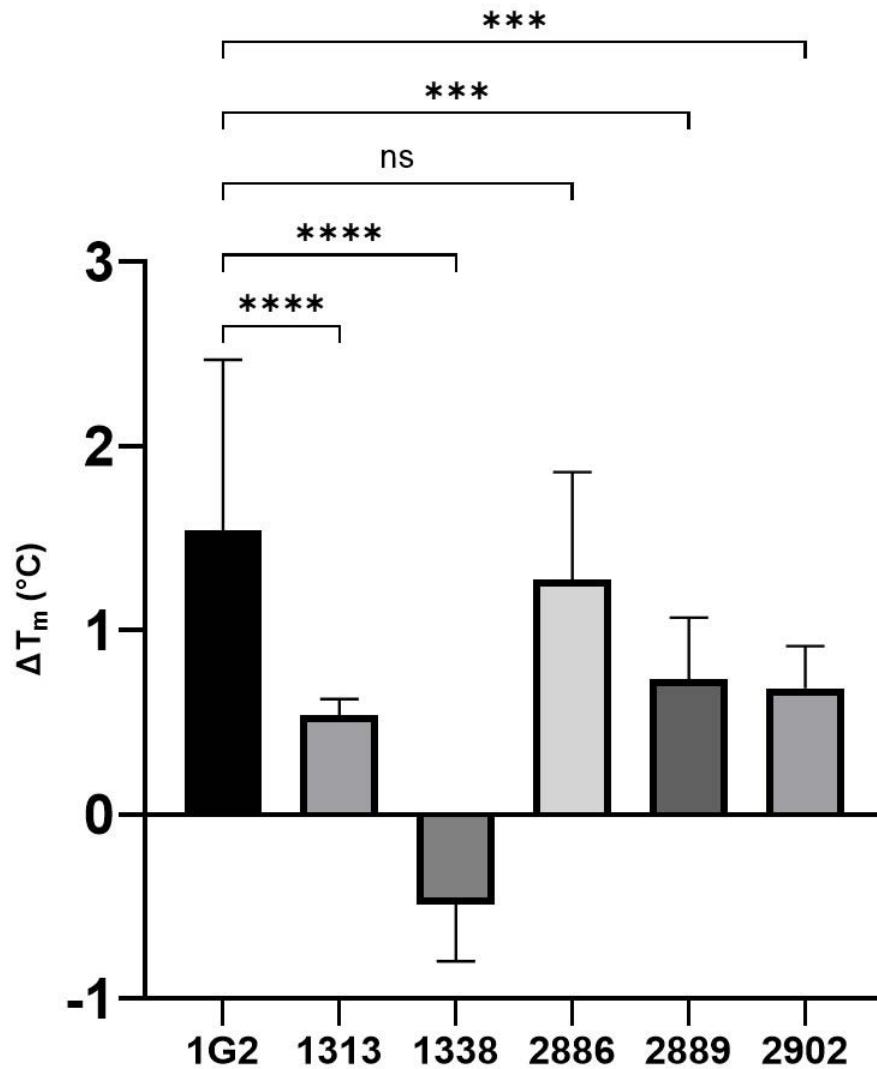


Figure 5. Melting temperature of Caga in the presence of ligands. Melting temperatures for Caga were determined using differential scanning fluorimetry (DSF). ANOVA test, ns ; non significant, *** $p < 0.001$, **** $p < 0.0001$

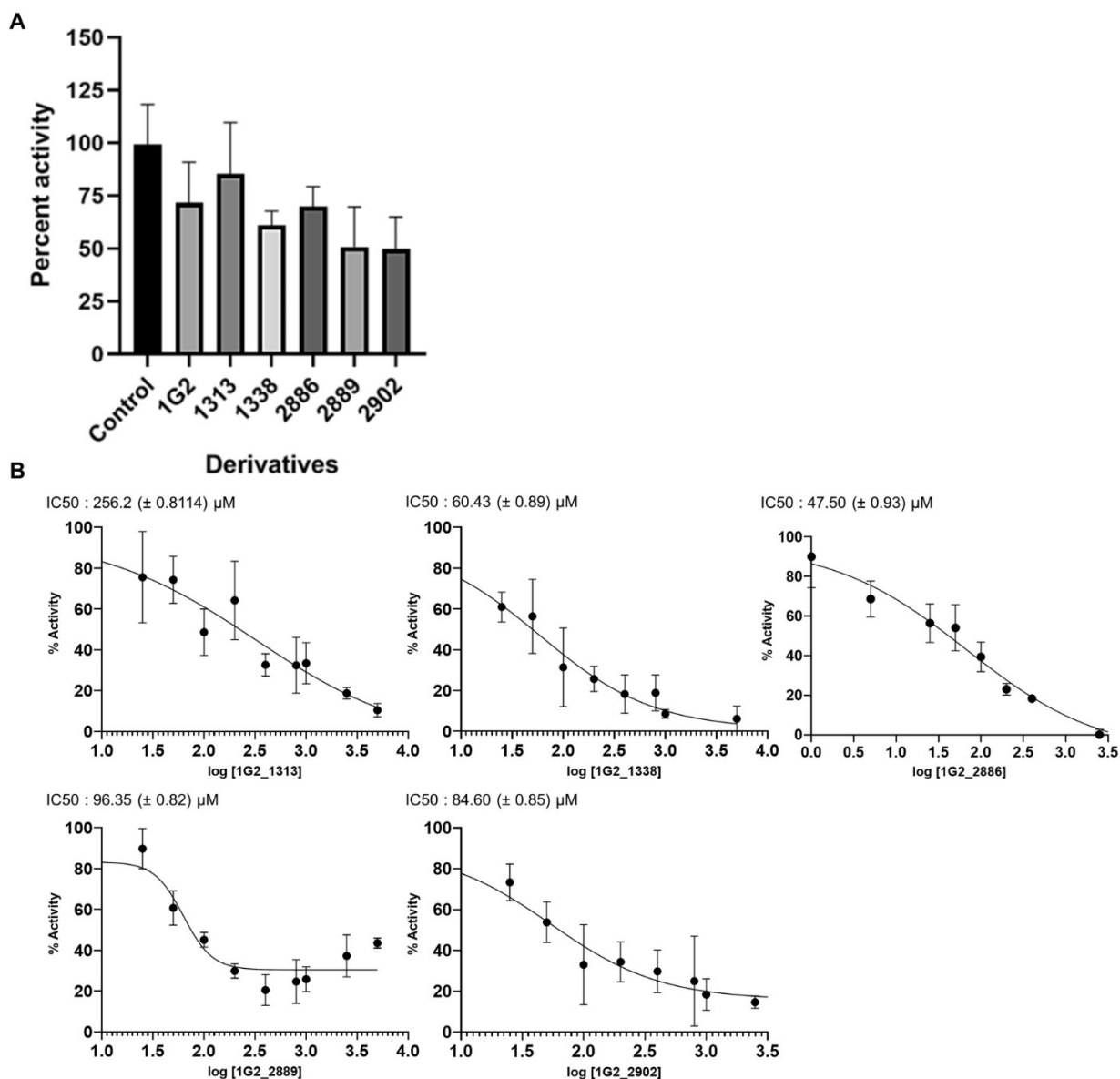


Figure 6. Enzyme assays of Cag α in the presence of molecule 1G2 and derivatives. A)

Inhibition of ATPase activity of Cag α in the presence of 500 μ M concentration of molecules, representation of one triplicate assay. B) Dose-response curves of ATPase activity showing IC₅₀ values in the presence of 1G2 and its derivatives 1G2_1313, 1G2_1338, 1G2_2886, 1G2_2889 and 1G2_2902.

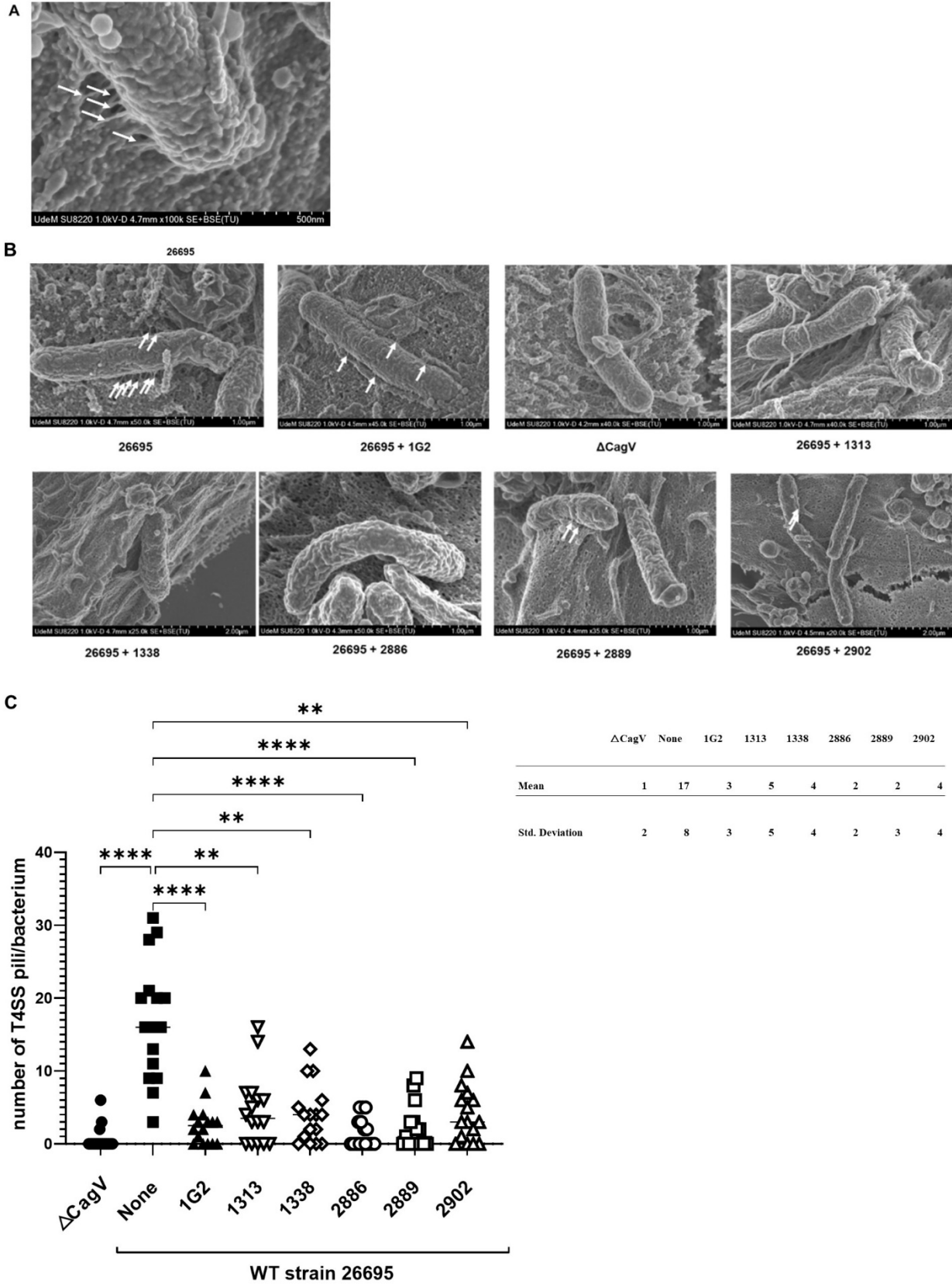


Figure 7: 1G2 and its derivatives affect the number of T4SSpili during gastric cell infection.

AGS cells were preincubated with 1G2 and derivatives and infected with *H. pylori*. A) and B) The T4SSpili were observed using scanning electron microscopy; the T4SS pili are identified with white arrows. C) The T4SS pili were counted using ImageJ. The $\Delta cagV$ strain was used as negative control. (n=16 bacteria from 2 different infections). ****: $p < 0.0001$, ** $p < 0.05$, ns: non-significant, Kruskal-Wallis ANOVA test

Tables

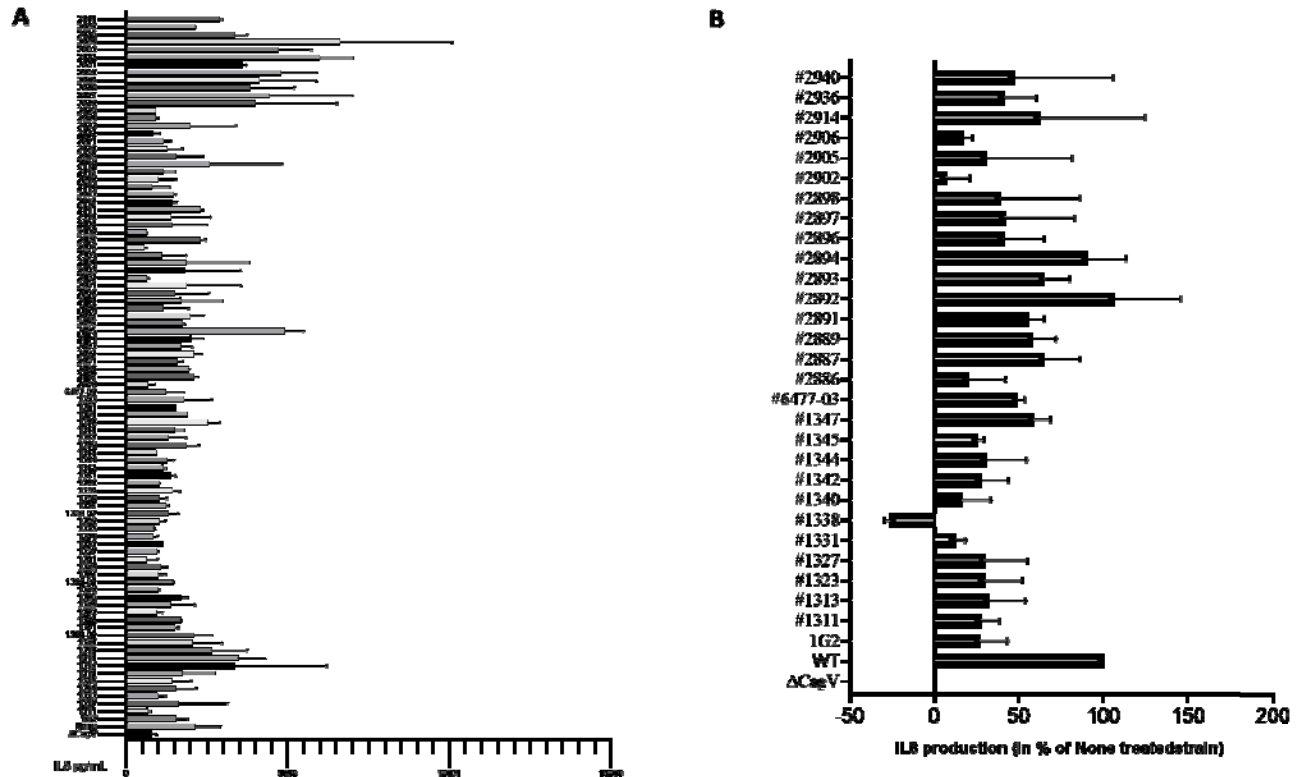
Name of compound	Structure
1G2 (4-(Pyrid-2-yloxy)benzoic acid)	
1313 4-[(5-acetamidopyridin-2-yl)oxy]benzoic acid	
1338 methyl 4-[(6-methylpyridin-2-yl)oxy]benzoate	
2886 2-chloro-4-[(6-methylpyridin-2-yl)oxy]benzoic acid	
2889 2-chloro-4-[(4-methylpyridin-2-yl)oxy]benzoic acid	
2902 3-[(4-methylpyridin-2-yl)oxy]benzoic acid	

Table 1: Structures of 1G2 derivatives identified by screening for potency in AGS cell infection assays.

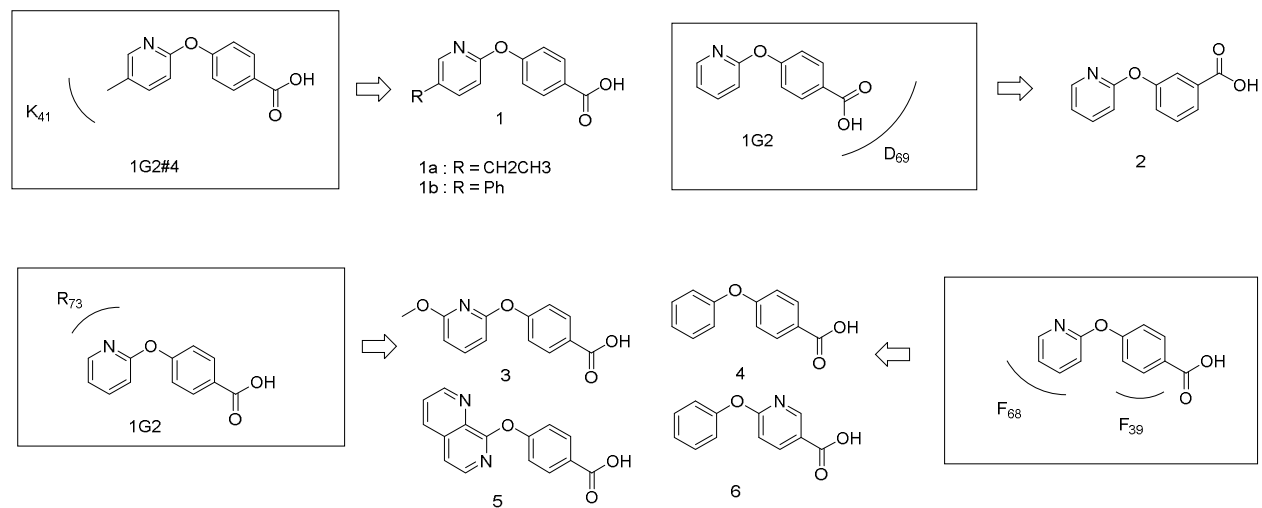
Supplementary information

H.pylori_Cag alpha	MTEDRLSAEDKKFLE-VERALKEAALNPLRHATEELFGDFLKMENITEICYNGNKVVVWL	59
A.tumefaciens_VirB11	-----ME---VDPQLRIILKPILEWLDDPRTEEVAINRPGAEAFVR	37
B.suis_VirB11	-----MMSNRSDFIVPDEAAVK---RAASVNFHLEPLRPWLDDPQITEVCVNRPGVEVFC	52
pKM101_traG	-----MTDAAFYQLGPLREYLEDDPTVFEIRINCFQEVICD	35
R388_TrwD	-----MSTVSKASPLSSGNRVG---KDQAVAQLLRPLDRFLDAPVTELSICRPGEVWTK	52
	: : * . * :	
H.pylori_Cag alpha	KNGGEWQPFDVDRDKAFSLSRMLHFARCCASFKKKTIDNYENPILSSNLANGERVQIVLS	119
A.tumefaciens_VirB11	Q-AGAFLKFLPV-S---YDDLEDIAILAGALRKQDV-GPRNPLCATELPGERLQICLP	91
B.suis_VirB11	R-ASAWEYVAVPNLD---YEHLISLGTATARFVDQDI-SDSRPVL SAILPMGERIQIVRP	107
pKM101_traG	T-FSGRRVQNAAIT---ADFIRNLAKSLVSS---NK-LTMQAINDVILPGGIRGVICLP	87
R388_TrwD	T-FEGWQVHEVPELT---EPFLQALITAIIVY---NG-VAPKSVNYVVLPGGQRGTIAQA	104
	: : : * * * *	
H.pylori_Cag alpha	PVTVNDETISISIRIPSKTTPHSEFEEQGFYNLLD-----	155
A.tumefaciens_VirB11	PT-VPSGTVSLTIRRPSRVSSSLKEVSSRYDAPRWNQWKERK-----KRH	135
B.suis_VirB11	PA-CEHGTISVTVIRKPSFTRRITLEDYAAQGGFFKHVRPMSK-----SL	148
pKM101_traG	PA-VIDGTTAVAFRKLAAADKNLEQLTSEGIFSDCRKITGSKQSLTDDDFFL-----	138
R388_TrwD	PA-VIDGTL SFLIRKHSLVVKTLEELDAEGAFDTFTDVSNKPSAEENHYLTVQDFTRL	163
	* . * : : *	
H.pylori_Cag alpha	-NKEQA-----ISAIKDGIAGKNVIVCGGTGSGKTTYIKSIMEFIPKEERIISI	204
A.tumefaciens_VirB11	DQHDEALLRYYDNGDLEAFLHACVVGRLTMLLCGPTGSGKTTMSKTLINAIPPQERLITI	195
B.suis_VirB11	TFPEQELLALKEAGDYSFLRRRAVQLERVIVVAGETGSGKTTLMKALMQEIPFDQLRITI	208
pKM101_traG	-----KELHSSEKWPAPFLQTAVEKKRTIVICGETGSGKTVLTRALLKSLHKDERVIL	191
R388_TrwD	EPFEVELLKLKRDGTIREFLEKCVLYKRNIIIAGKTGSGKTTFARSLIEKVPPEERIITI	223
	: . : : : * * * * * . : : : : : : * * * :	
H.pylori_Cag alpha	EDTEELVFKHHKNYQLFFGGN-----ITSADCLKSCLRMRPDRIILGELRSSEAYD	256
A.tumefaciens_VirB11	EDTLELVIPH-ENHVRLLYSKNGA--GLGAVTAEHLLQASLRMRPDRILLGEIRDDAAWA	252
B.suis_VirB11	EDVPELFLPDHPNHVHLFYPSEAKEEENAPVTAATLLRSCLRMKPTRILLAEIRGGEAYD	268
pKM101_traG	EDVHEVTVDHVVEAVYMMYGDAGK---IGPVSATDALRACMRLTPGRIIMTELRDDAAWD	248
R388_TrwD	EDVHELFLPNHPNRVHMLYGYG----AGRVSADECLAACMRQSPDRIFLAEIRGNEAWE	278
	** . * : . . . : : : : : : : * : : * * * : : * : * : * :	
H.pylori_Cag alpha	FYNVLCSGHGKTLTTLHAGSSEAFIRLANMSSSNSAARNIKFESLIEGFKDLIDMIVHI	316
A.tumefaciens_VirB11	YLSEVVSQHGPGSISTIHGANPVQGFKKLFLSVKSSAQGASLEDRTLIDMLATAVDVIVPF	312
B.suis_VirB11	FINVAASGHGGSITSCHAGSCELTFFERLALMVLQNRQGRQLPYEIRRLLYLVVDVVVHV	328
pKM101_traG	YLKALNTGHPGGVMSTHANSARDAFNRIIGLLIKATPIGRMLDMSD IMRMLYSTIDVVVHM	308
R388_TrwD	YLNLSLNTGHPGSITTHANNALQTFERCATLIKKSVDVGRQLEMEMIKLVLYTTIDVVLFF	338
	: . : * * * : : * . * : : . . : : : : * : : :	
H.pylori_Cag alpha	NHH-----KQCDEFYIKHR-----	330
A.tumefaciens_VirB11	RA---HGDIVEVGEIWLAAADARRRGETIGDLLNQ	344
B.suis_VirB11	HNGVHDGTGRHISEVVYDPNTRKALS-LQHSEKT-	361
pKM101_traG	E-----RKKIKEIYFDPEYKMQCV-NGSL----	331
R388_TrwD	K-----DKLVEVFYDPIFSKSKM-A-----	358
	. . * . :	

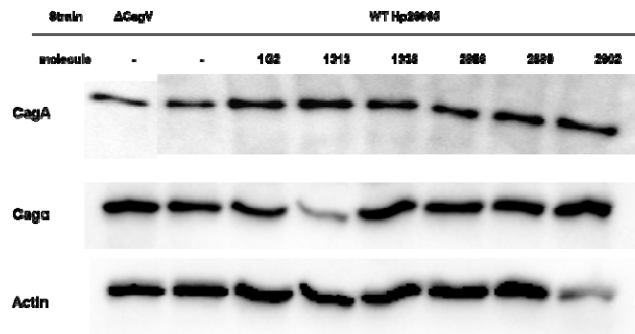
supplementary Figure 1. Multiple sequence alignment of Caga/VirB11 homologs. Selected Caga/VirB11 homologs from the T4SS of *Agrobacterium tumefaciens* C58, *Brucella suis* 1330, plasmids pKM101 and R388 were aligned using the clustal omega online tool (<https://www.ebi.ac.uk/Tools/msa/clustalo/>). The amino acids corresponding to the 1G2 binding site on Caga are indicated in red and the ATPase active site is labelled green with a box.



supplementary Figure 2: Results of the screens of 1G2 derivatives. AGS cells were infected for 24h with *H. pylori* pre-incubated with 200 μ M of molecules and the amounts of secreted IL-8 were measured by ELISA A) first screening results in pg/mL, B) The results of the IL-8 quantification were analyzed by pairs comparing the non-treated result (100% induction) with the treated results. The $\Delta cagV$ strain was used as negative control and analyzed using the strain 26695.



supplementary Figure 3: Design of 1G2 analogs. Overview of the synthetic analogs designed to probe the putative interactions between the 1G2 derivatives and the various amino acids at the binding site.



supplementary Figure 4: Expression of Cag protein during AGS cells infection with or without treatment with 1G2 and its derivatives. Cell lysates of *H. pylori* strains were separated by SDS-PAGE, followed by western blotting with specific antisera. CagA and Cagα proteins were detected using specific antibodies and actin was used as a loading control. Representative results from four repetitions are shown.

supplementary Table 1: Primers for the creation of 1G2 binding site mutants

PRIMER'S NAME	CODON	AA	PRIMER 5' to 3'
cagalpha_D38A_F	GAT->GCG	D38A	GAAGAACTTTTTGGTGCGTTTTTAAAAATGGAA
cagalpha_D38A_R			TTCCATTTTTAAAAACGCACCAAAAAGTTCTTC
cagalpha_F39A_F	TTT->GCG	F39A	GAACTTTTTGGTGATGCGTTAAAAATGGAAAAT
cagalpha_F39A_R			ATTTTCCATTTTTAACGCATCACCAAAAAGTTC
cagalpha_K41A_F	AAA->GCG	K41A	TTTGGTGATTTTTTAGCGATGGAAAATATCACT
cagalpha_K41A_R			AGTGATATTTTCCATCGCTAAAAAATCACCAA
cagalpha_M42A_F	ATG->GCG	M42A	GGTGATTTTTTAAAAGCGGAAAATATCACTGAG
cagalpha_M42A_R			CTCAGTGATATTTTCCATTTTTTAAAAAATCACC
cagalpha_F68A_F	TTT->GCG	F68A	GGCGAATGGCAACCAGCGGATGTGAGAGACAGG
cagalpha_F68A_R			CCTGTCTCTCACATCCGCTGGTTGCCATTGCGC
cagalpha_R73A_F	AGG->GCG	R73A	CAGGCTAAAGGCTTTCGCGTCTCTCACATCAAA
cagalpha_R73A_R			TTTGATGTGAGAGACGCGAAAGCCTTTAGCCTG
cagalpha_R73K_F	AGG->AAA	R-73K	CAGGCTAAAGGCTTTTTTGTCTCTCACATCAAA
cagalpha_R73K_R			TTTGATGTGAGAGACAAAAAAGCCTTTAGCCTG

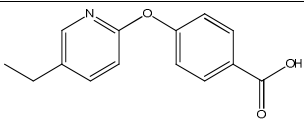
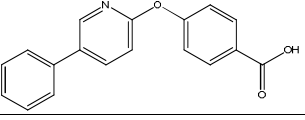
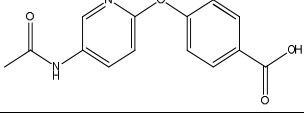
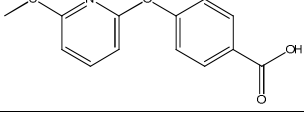
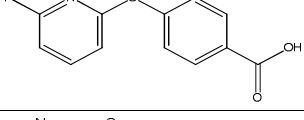
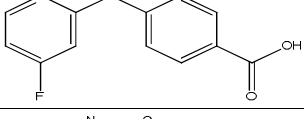
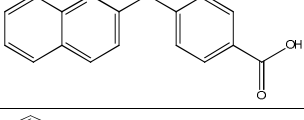
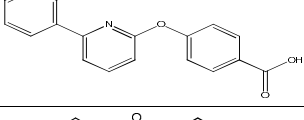
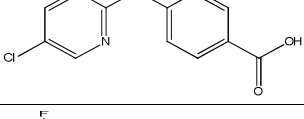
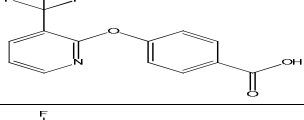
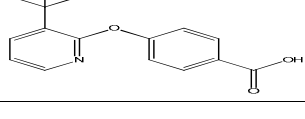
supplementary Table 2: X-ray data collection and refinement statistics.

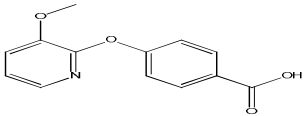
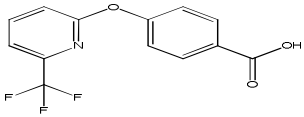
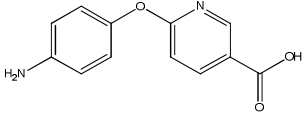
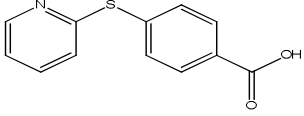
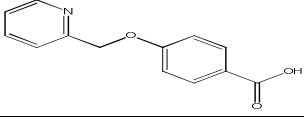
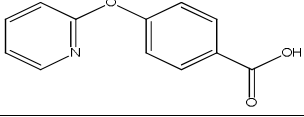
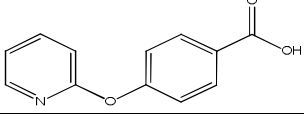
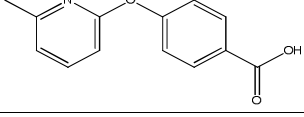
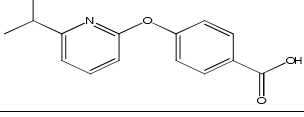
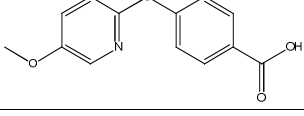
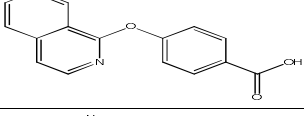
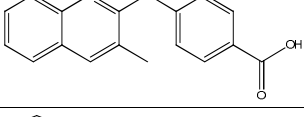
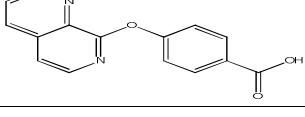
□	Cagα-1G2
Resolution range	38.5 - 2.9 (3.00 - 2.90)
Space group	<i>P</i> 6 ₃ 22
Unit cell	112.075 112.075 231.006 90 90 120
Total reflections	165306
Unique reflections	18083 (1737)
Multiplicity	5.2
Completeness (%)	92.4 (90.74)
Mean I/sigma(I)	7.4(2.4)
Wilson B-factor	45.43
R-merge	0.12
R-pim	0.08
Reflections used in refinement	18049 (1734)
Reflections used for R-free	976 (92)
R_{work} / R_{free}	0.230 (0.313) / 0.278 (0.423)
Protein residues	646
RMS (bonds)	0.012
RMS (angles)	1.59
Ramachandran favored (%)	95.1
Ramachandran allowed (%)	4.59
Ramachandran outliers (%)	0.31
Clashscore	3.87
Average B-factor	46.27
Coordinate error	0.203
PDB	6BGE

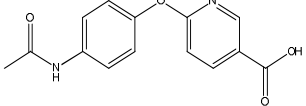
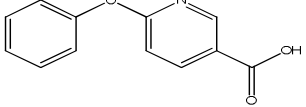
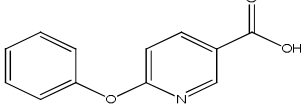
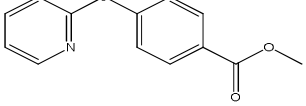
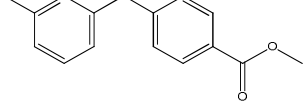
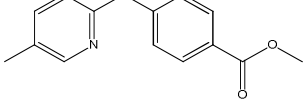
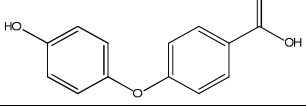
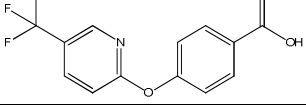
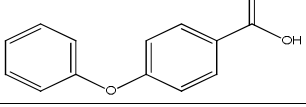
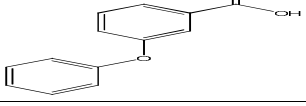
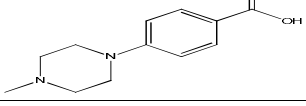
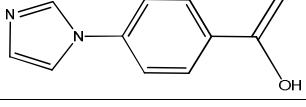
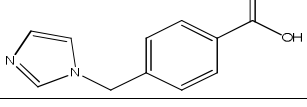
supplementary Table 3: Docking of derivatives of molecule 1G2 with target CagA. Binding energy is shown as kmol/mol as calculated by Autodock Vina software.

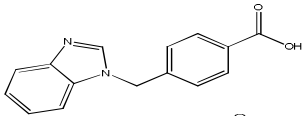
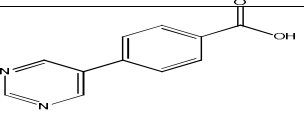
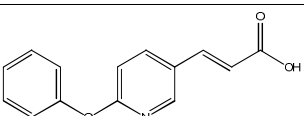
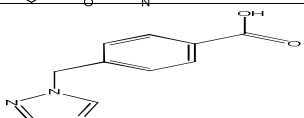
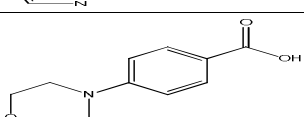
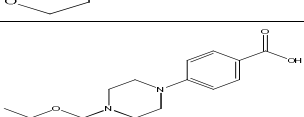
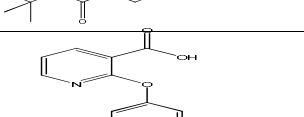
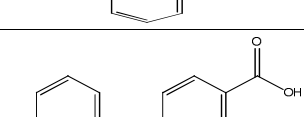
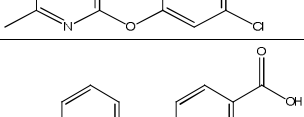
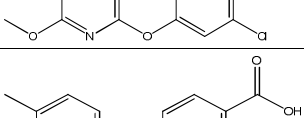
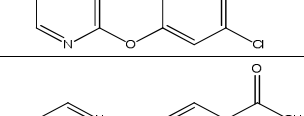
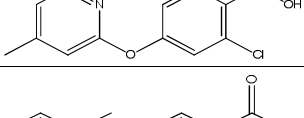
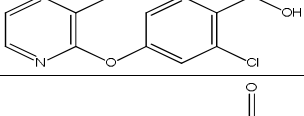
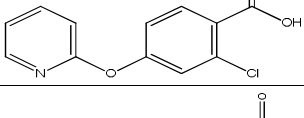
Molecule	Binding energy ($\Delta G/mol$)
1G2	-6.6
1G2_1313	-10.2
1G2_1338	-9.0
1G2_2886	-9.4
1G2_2889	-9.4
1G2_2902	-9.6

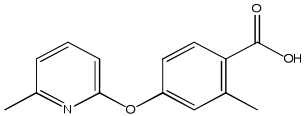
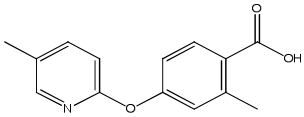
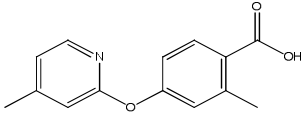
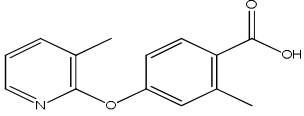
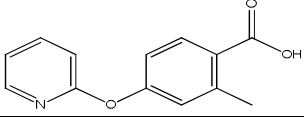
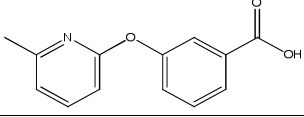
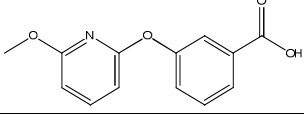
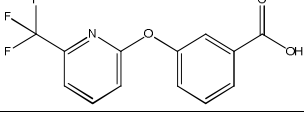
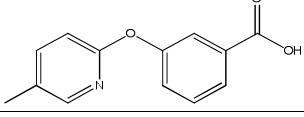
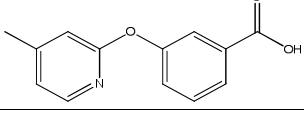
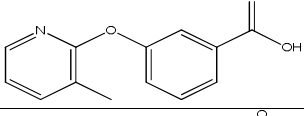
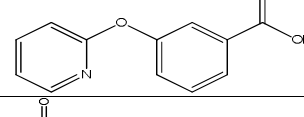
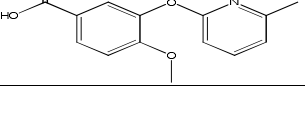
supplementary Table 4: List of 1G2 derivatives created by medicinal chemistry. Structures, composition, names assigned after synthesis, numbers, AGS cell cytotoxicity and inhibition of *H. pylori* 26696 growth.

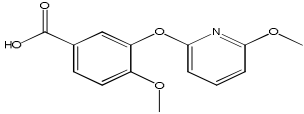
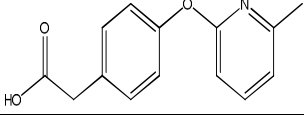
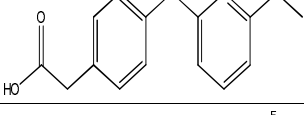
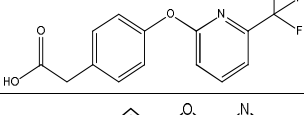
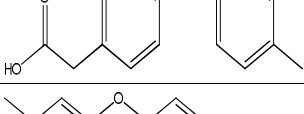
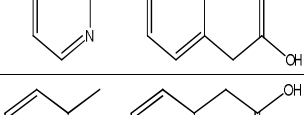
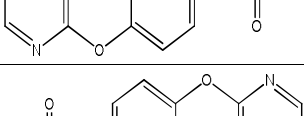
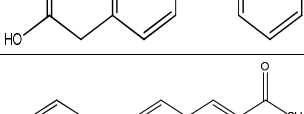
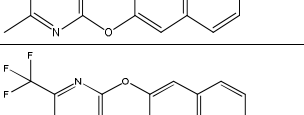
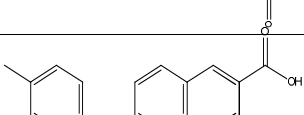
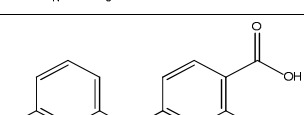
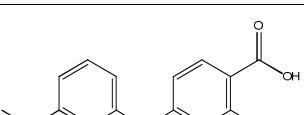

Structure	Composition	UM#	Name of the molecule	Cells cytotoxicity	26695 growth inhibition
	C14H13NO3	UM0141311-01	#1311	None	None
	C18H13NO3	UM0141312-01	#1312	None	None
	C14H12N2O4	UM0141313-01	#1313	None	None
	C13H11NO4	UM0141314-01	#1314	None	None
	C12H8FNO3	UM0141315-01	#1315	None	None
	C12H8FNO3	UM0141316-01	#1316	None	None
	C16H11NO3	UM0141317-01	#1317	None	None
	C18H13NO3	UM0141318-01	#1318	None	None
	C12H8ClNO3	UM0141319-01	#1319	None	None
	C13H8F3NO3	UM0141320-01	#1320	None	None
	C13H8F3NO3	UM0141320-02	#1320-02	None	None

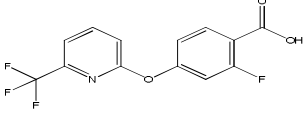
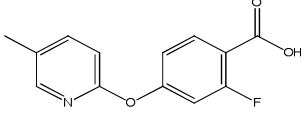
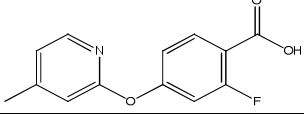
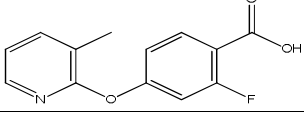
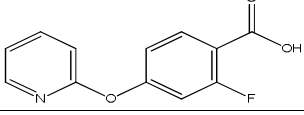
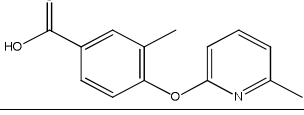
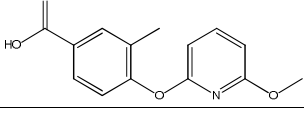
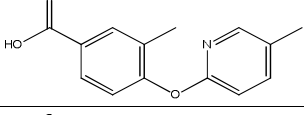
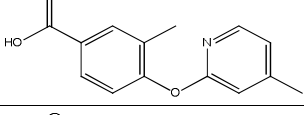
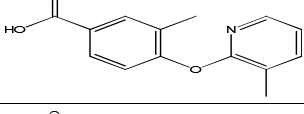
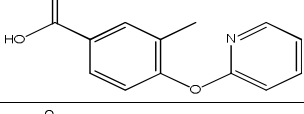
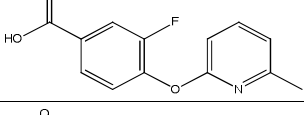
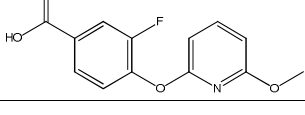
	C13H11NO4	UM0141321-01	#1321	None	None
	C13H8F3NO3	UM0141322-01	#1322	None	None
	C12H10N2O3	UM0141323-01	#1323	None	None
	C12H9NO2S	UM0141324-01	#1324	None	None
	C13H11NO3	UM0141325-01	#1325	None	None
	C12H9NO3	UM0141326-01	#1326	None	None
	C12H9NO3	UM0141326-02	#1326-02	None	None
	C13H11NO3	UM0141327-01	#1327	None	None
	C15H15NO3	UM0141328-01	#1328	None	None
	C13H11NO4	UM0141331-01	#1331	None	None
	C16H11NO3	UM0141332-01	#1332	None	None
	C17H13NO3	UM0141333-01	#1333	None	None
	C15H10N2O3	UM0141334-01	#1334	None	None

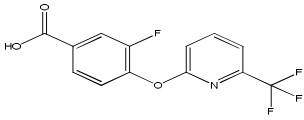
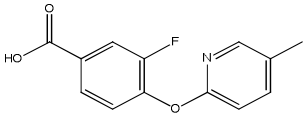
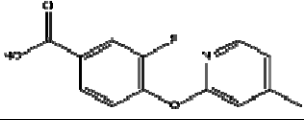
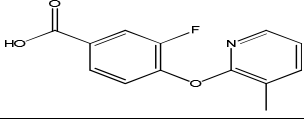
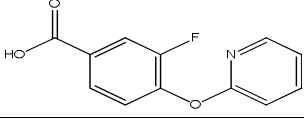
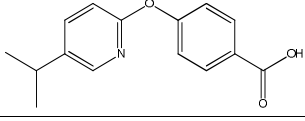
	C14H12N2O4	UM0141335-01	#1335	None	None
	C12H9NO3	UM0141336-01	#1336	None	None
	C12H9NO3	UM0141336-02	#1336-02	None	None
	C13H11NO3	UM0141337-01	#1337	None	None
	C14H13NO3	UM0141338-01	#1338	None	None
	C14H13NO3	UM0141339-01	#1339	None	None
	C13H10O4	UM0141340-01	#1340	None	None
	C13H8F3NO3	UM0141341-01	#1341	None	None
	C13H10O3	UM0141342-01	#1342	None	None
	C13H10O3	UM0141343-01	#1343	yes	None
	C12H16N2O2	UM0141344-01	#1344	None	None
	C10H8N2O2	UM0141345-01	#1345	None	None
	C11H10N2O2	UM0141346-01	#1346	None	None

	C15H12N2O2	UM0141347-01	#1347	None	None
	C11H8N2O2	UM0141348-01	#1348	None	None
	C14H11NO3	UM0141349-01	#1349	None	None
	C10H9N3O2	UM0141350-01	#1350	None	None
	C11H13NO3	UM0141351-01	#1351	None	None
	C16H22N2O4	UM0141353-01	#1353	None	None
	C12H9NO3	UM0016477-03	#6477-03	None	None
	C13H10ClNO3	UM0142886-01	#2886	None	None
	C13H10ClNO4	UM0142887-01	#2887	None	None
	C13H10ClNO3	UM0142888-01	#2888	yes	None
	C13H10ClNO3	UM0142889-01	#2889	none	None
	C13H10ClNO3	UM0142890-01	#2890	Yes	None
	C12H8ClNO3	UM0142891-01	#2891	none	None
	C12H7F3N2O3	UM0142892-01	#2892	none	None

	C14H13NO3	UM0142893-01	#2893	none	None
	C14H13NO3	UM0142894-01	#2894	none	None
	C14H13NO3	UM0142895-01	#2895	none	None
	C14H13NO3	UM0142896-01	#2896	none	None
	C13H11NO3	UM0142897-01	#2897	none	None
	C13H11NO3	UM0142898-01	#2898	none	None
	C13H11NO4	UM0142899-01	#2899	none	None
	C13H8F3NO3	UM0142900-01	#2900	none	None
	C13H11NO3	UM0142901-01	#2901	none	None
	C13H11NO3	UM0142902-01	#2902	none	None
	C13H11NO3	UM0142903-01	#2903	none	None
	C12H9NO3	UM0142904-01	#2904	none	None
	C14H13NO4	UM0142905-01	#2905	none	None

	C14H13NO5	UM0142906-01	#2906	none	None
	C14H13NO3	UM0142907-01	#2907	none	None
	C14H13NO4	UM0142908-01	#2908	none	None
	C14H10F3NO3	UM0142909-01	#2909	none	None
	C14H13NO3	UM0142910-01	#2910	none	None
	C14H13NO3	UM0142911-01	#2911	none	None
	C14H13NO3	UM0142912-01	#2912	none	None
	C13H11NO3	UM0142913-01	#2913	none	None
	C17H13NO3	UM0142914-01	#2914	none	None
	C17H10F3NO3	UM0142915-01	#2915	yes	None
	C17H13NO3	UM0142916-01	#2916	None	None
	C13H10FNO3	UM0142917-01	#2917	None	None
	C13H10FNO4	UM0142918-01	#2918	None	None

	C13H7F4NO3	UM0142919-01	#2919	None	None
	C13H10FNO3	UM0142920-01	#2920	None	None
	C13H10FNO3	UM0142921-01	#2921	None	None
	C13H10FNO3	UM0142922-01	#2922	None	None
	C12H8FNO3	UM0142923-01	#2923	None	None
	C14H13NO3	UM0142924-01	#2924	None	None
	C14H13NO4	UM0142925-01	#2925	None	None
	C14H13NO3	UM0142926-01	#2926	None	None
	C14H13NO3	UM0142927-01	#2927	None	None
	C14H13NO3	UM0142928-01	#2928	None	None
	C13H11NO3	UM0142929-01	#2929	None	None
	C13H10FNO3	UM0142930-01	#2930	None	None
	C13H10FNO4	UM0142931-01	#2931	None	None

	C13H7F4NO3	UM0142932-01	#2932	None	None
	C13H10FNO3	UM0142933-01	#2933	None	None
	C13H10FNO3	UM0142934-01	#2934	None	None
	C13H10FNO3	UM0142935-01	#2935	None	None
	C12H8FNO3	UM0142936-01	#2936	None	None
	C15H15NO3	UM0142940-01	#2940	None	None